CrossMark

Studying the effect of material initial conditions on drying induced stresses

M. Heydari[1] · K. Khalili[1] · S. Y. Ahmadi-Brooghani[1]

Abstract Cracking as a result of non-uniform deformation during drying is one of defects that may occur during drying and has to be dealt with by proper drying treatment. In the current study the effect of initial condition has been investigated on stress-strain induced by drying. The convective drying of a porous clay-like material has been simulated by using a mathematical model. Mass and heat transfer along with the mechanical behavior of the object being dried make the phenomenon a highly coupled problem. The coupling variables are the solid displacement, moisture content and temperature of the porous medium. A numerical solution is sought and employed to predict the influence of initial conditions of material on the drying induced stresses, the moisture content, and the temperature variations. Simulation results showed that increasing the initial temperature is an effective way to reduce the stresses induced by drying and to obtain products with good quality without significant change in drying curve and in comparison this is more effective than intermittent drying.

1 Introduction

Drying is a simultaneous mass and heat transfer processes in which moisture from porous Clay-like material is removed. Drying operation consumes about 20% of national industrial

energy [1]. Producing good quality products while maintaining the energy consumption and cost at the lowest possible level is the main objective of most industrial drying operation. Long drying time and severe drying condition can significantly decrease the product quality; e.g., by color change [2], deformation (shrinkage) and cracks which are mainly caused by non-uniform shrinkage [3]. Avoiding the problems mentioned necessitates establishment of a more realistic mathematical model and precise design of drying condition. Generally, the drying process modeling is composed of the equations of mass, heat, and momentum conservation forming a system of partial differential equations. Thermal, moisture, and mechanical properties changes interaction with conservation equations make the drying process modeling complex [4].

Moisture transfer in porous materials can be accomplished by several transport mechanisms, such as moisture diffusion due to concentration gradients, Thermo diffusion, Knudsen diffusion, capillary flow, evaporation and condensation [5]. Although all these transport mechanisms have a strong physical basis the moisture diffusion is the most important mechanism of mass transport [6]. The mass transfer rate by diffusion is proportional to the moisture gradient of the moisture content which is expressed by Fick's equation.

Taking all of the transport mechanisms in the drying process into consideration makes a very complex problem rendering the solution infeasible. Furthermore, in many situations, it is not required/applicable to consider all mechanisms. The most common approach in engineering applications to overcome the problem and to take into account the relevant mechanisms is to lump all effects of the transport mechanisms onto the diffusion coefficient in Fick's law.

Thus, the diffusion coefficient becomes an effective coefficient. In this study the diffusive model based on the phenomenon of diffusion described by Fick's law was used for the description of moisture movement. Fick's law with an effective

✉ K. Khalili
  kkhalili@birjand.ac.ir

  M. Heydari
  m.heydari@birjand.ac.ir

  S. Y. Ahmadi-Brooghani
  s.y.ahmadi@birjand.ac.ir

[1] University of Birjand, Birjand, Iran

diffusion coefficient has already been used successfully by many authors in mathematical model of drying process [6–10].

The material properties of the product may change during drying. Considering the variation of physical and mechanical properties of deformable media during drying is essential for mathematical modeling. The added complexity of identification and consideration of the material properties variations obliged a wide range of study to use constant parameters in the models dealing with drying [11–13]. Indeed, most products cannot really fit into this simple model and need complex models which take into account the variation of many parameters (Young modulus, diffusion coefficient, density, etc.) with moisture content and temperature. The material properties variation during drying has been considered in this study.

Non-uniform distribution of moisture and temperature are not uncommon in most of material when drying. Gradient of moisture and temperature from the surface to the core is responsible for high tensile stresses. Usually the stresses are compressive in the inner part of the material and tensional on the surface layers. Numerical investigation of the drying stresses dates back to 1970s [14]. If the stresses induced by drying process exceed the critical strength of the material, the clay cracks. Crack formation often, makes the dried products useless. Drying induced stresses depends on many parameters which can be classified into three major groups as follows: drying conditions, Material's properties, and initial condition of material.

There are a large number of research works studying the effect of drying conditions on drying induced stresses [15–17]. Banaszak and Kowalski have presented a study which investigates the effect of drying condition on the stresses responsible for crack formation [18]. Musielak determined the moisture, and temperature distributions, and stresses- strains induced by drying for different drying conditions [19]. Using a finite element method Manel et al. simulated intermittent convective drying [20]. They showed that moisture stress fields reduced when compared to continuous heating. Some authors have suggested a stress base criterion which can be used to predict the crack formation during the drying process. When this criterion is introduced the drying conditions range can be increased under which the materials cracking is avoided [21, 22]. Pourcel et al. investigated crack initiation time during drying and stated that it depends on the drying rate [23].

A number of studies can be found in the literatures dealing with the influence of Material's properties on drying kinetic [2, 24] and drying induced stresses. Musielak and Sliwa showed that the clay quartz content affects the severity of cracking [25]. Surveying the literature reveals that there is not published works on the effect of initial conditions on drying induced stresses.

The current study addresses the conjugate problem of heat and mass transfer and the resulting stresses. The influence of initial conditions on the stresses induced by drying is studied in a clay sample. The results are analyzed and discussed.

2 Classical periods of drying

Convective drying process presents three classical periods as follow: preheating period, constant drying rate period (CDRP) and falling drying rate period (FDRP) (Fig. 1). In the preheating period the material with the initial temperature (T_o) starts to heat up/down to the wet bulb temperature (F-J or G-J) and consequently the drying rate starts to drop/rise (A-C or B-C) [26]. The CDRP begins at time t_w as shown in Fig. 1. At this point; the material temperature is equal to the wet bulb temperature (J) and remains constant (J-K). A film of water is available at the exchange surface during the CDRP hence it is fully governed by the external heat and mass transfer rates. The moisture migrates from the interior of the material to the exchange surface by diffusion of liquid water [27] and the moisture diffusion coefficient is almost constant [28]. The drying rate remains constant as long as the moisture transport rate from the interior of the material to the exchange surface can withstand the evaporation rate from the exchange surface (C-D).

The CDRP is almost independent of the material being dried, however; many products, behave differently not displaying the CDRP at all, since the rate at which water becomes accessible at the exchange surface is determined by internal mass and heat transfer rates [8, 29]. The ending point of the CDRP is called the critical moisture content point (D).

The FDRP (D-E) begins from time t_c during which time a reduction in drying rate occurs. The internal moisture transport rate specifies the drying rate of the FDRP.

The temperature of material surpasses the wet bulb temperature and grows up to the drying air temperature (K-L). Finally, the drying process stops when the equilibrium moisture content (E) reaches.

Usually the maximum moisture and temperature non-uniformity occurs at the end of the CDRP [30] hence material cracking is most possible to happen at this stage of drying [6,
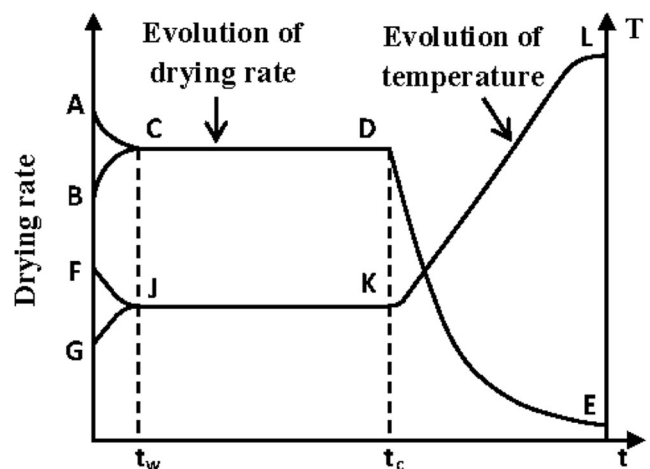

Fig. 1 dependence of moisture content and temperature on drying time

20]. This is the reason why a large body of study are devoted to the CDRP [31–33].

3 Dew point and wet bulb temperature

During the CDRP the material temperature is equal to the wet bulb temperature [26]. influenced by the heat and mass transfer rates [34]. It can be written by the following eq. [35]:

$$
\begin{aligned}
T_w = Tatan&\left[0.151977(RH\% + 8.313659)^{1/2}\right] \\
&+ atan(T + RH\%) - atan(RH\% - 1.676331) \\
&+ 0.00391838(RH\%)^{3/2}atan(0.023101RH\%) - 4.686035
\end{aligned} \quad (1)
$$

If the sample's initial temperature be lower than the dew point temperature of the chosen air conditions, the water vapor condenses onto the sample's surfaces. Consequently, the moisture content increases and material swelling occurs at the beginning of drying.

4 Shrinkage effects on drying behavior

Most of materials shrink during drying. The amount and intensity of material shrinkage depend on their properties and drying condition [36]. Shrinkage or solid displacement is one of the most important coupling variables in system of equation described in next sections. Shrinkage has strong effect on drying behavior of highly shrinkable porous media and causes the change of the drying surface and as a consequent the drying rate. Drying rate has direct effect on the drying time and intensity of the non-uniform distribution of the moisture content and temperature, and consequently on the intensity of drying induced stresses.

Many studies assumed the shrinkage of the material being dried is equal to the volume of the evaporated moisture (moisture strain) during the two first phases of drying [7, 20, 37, 38] and neglected mechanical strains (ideal shrinkage) [39] which is introduced by drying induced stresses. To calculate mechanical strains, the momentum balance equations need to be considered in mathematical model.

The shrinkage is the main aspect of drying process. Although the shrinkage is a key coupling variable in system of drying eq. [22] and must be incorporated in mathematical model in order to accurately simulate the drying process, there is a large body of literatures that neglect shrinkage [40].

In the current study the moisture and mechanical strains which are generally the main strain constituents in drying [41] are taken into account. Also the mean moisture content evolution of material, with and without including the shrinkage effect has been illustrated.

5 The mathematical model

The mathematical model of the drying process is presented in this section. The particularity of the model is that it considers the strong coupling between heat transport, mass transport, and the mechanical behavior of the material. The model takes into account the shrinkage through the mechanical behavior of the material that is assumed to be and remain elastic. In the mathematical model, the following assumptions are taken into account:

- Clay is a homogeneous and isotropic porous material.
- Gaseous phase and gravitational effect are neglected.
- Local thermal equilibrium is assumed.
- The material assumed to behave elastic.

With regard to the assumptions, the equations which describe heat and mass transfer aspects of drying are taken into account in the following form:

$$
\frac{\partial w}{\partial t} = \nabla.(D\nabla w) \quad (2)
$$

$$
\rho C_p \frac{\partial T}{\partial t} = \nabla.(\lambda \nabla T) \quad (3)
$$

The momentum balance equation is considered as follow:

$$
\nabla.\sigma = 0 \quad (4)
$$

The volume variation depends on the changes of temperature and moisture content while the material deformation is assumed to be small. Therefore, by subtracting the moisture and thermal strains (respectively ε^H and ε^T) from the total strain, mechanical strain can be obtained.

$$
\varepsilon^M = \varepsilon - \varepsilon^T - \varepsilon^H, \quad \varepsilon^T = \alpha(T - T_0), \quad \varepsilon^H = \beta(w - w_0) \quad (5)
$$

Here α is the thermal expansion and β is the moisture expansion coefficient. In the case of elastic behavior, the strain–stress relation is given as fallow:

$$
\varepsilon_x = \frac{\sigma_x}{E} - \nu\frac{\sigma_y}{E} - \nu\frac{\sigma_z}{E} + \alpha\Delta T + \beta\Delta W \quad (6)
$$

$$
\varepsilon_y = -\nu\frac{\sigma_x}{E} + \frac{\sigma_y}{E} - \nu\frac{\sigma_z}{E} + \alpha\Delta T + \beta\Delta W \quad (7)
$$

$$
\varepsilon_x = -\nu\frac{\sigma_x}{E} - \nu\frac{\sigma_y}{E} + \frac{\sigma_z}{E} + \alpha\Delta T + \beta\Delta W \quad (8)
$$

The above equations can be rewritten as fallow:

$$
\varepsilon_x = \frac{1}{E}\left(\sigma_x(1 + \nu) - \nu(\sigma_x + \sigma_y + \sigma_z)\right) + \alpha\Delta T + \beta\Delta W \quad (9)
$$

$$
\varepsilon_y = \frac{1}{E}\left(\sigma_y(1 + \nu) - \nu(\sigma_x + \sigma_y + \sigma_z)\right) + \alpha\Delta T + \beta\Delta W \quad (10)
$$

$$
\varepsilon_z = \frac{1}{E}\left(\sigma_z(1 + \nu) - \nu(\sigma_x + \sigma_y + \sigma_z)\right) + \alpha\Delta T + \beta\Delta W \quad (11)
$$

Consequently:

$$\varepsilon_x + \varepsilon_y + \varepsilon_z = \frac{1-2\nu}{E}\left(\sigma_x + \sigma_y + \sigma_z\right) + 3\alpha\Delta T$$
$$+ 3\beta\Delta W \tag{12}$$

so it comes:

$$\sigma_x = \frac{E\nu}{(1-2\nu)(1+\nu)}\left(\varepsilon_x + \varepsilon_y + \varepsilon_z\right)$$
$$+ \frac{E}{(1+\nu)}\varepsilon_x - \frac{E}{(1-2\nu)}\left((\alpha\Delta T + \beta\Delta W)\right) \tag{13}$$

$$\sigma_y = \frac{E\nu}{(1-2\nu)(1+\nu)}\left(\varepsilon_x + \varepsilon_y + \varepsilon_z\right)$$
$$+ \frac{E}{(1+\nu)}\varepsilon_y - \frac{E}{(1-2\nu)}\left((\alpha\Delta T + \beta\Delta W)\right) \tag{14}$$

$$\sigma_z = \frac{E\nu}{(1-2\nu)(1+\nu)}\left(\varepsilon_x + \varepsilon_y + \varepsilon_z\right)$$
$$+ \frac{E}{(1+\nu)}\varepsilon_z - \frac{E}{(1-2\nu)}\left((\alpha\Delta T + \beta\Delta W)\right) \tag{15}$$

The equation of 13, 14 and 15 can be simplifies as fallow:

$$\boldsymbol{\sigma} = \lambda tr(\varepsilon)\boldsymbol{I} + 2\mu\varepsilon - 3K\beta(w-w_0)\boldsymbol{I} - 3K\alpha(T-T_0)\boldsymbol{I} \tag{16}$$

$$K = \frac{E}{3(1-2\nu)}, \quad \lambda = \frac{E\nu}{(1-2\nu)(1+\nu)}, \quad \mu$$
$$= \frac{E}{2(1+\nu)} \tag{17}$$

Where K is the bulk modulus, μ and λ are the Lame constants.

6 Initial and boundary conditions

The moisture content and temperature are initially uniform:

$$t = 0, \quad T = T_0 \tag{18}$$
$$t = 0, \quad w = w_0 \tag{19}$$

The values of the parameters used in the simulations are given in Table 1. The mass and heat fluxes are expressed as fallow at the exchange surface:

$$-D_{eff}\nabla w = F_m \tag{20}$$
$$-k\nabla T = \mathrm{h}(\mathrm{T}_s - \mathrm{T}_{inf}) - h_v F_m \tag{21}$$

Where D_{eff} is effective diffusion coefficient, h_v is the latent heat of evaporation, h and k are convection and conduction

heat transfer coefficient respectively. F_m is the vaporization rate of the moisture at the exchange surface which is a function of surface temperature and relative humidity. F_m can be calculated by the following eq. [45]:

$$F_m = 13^* \quad 10^{-3*} \quad \left(C_{inf} - C_{surf}\right)$$
$$C_{inf} = \frac{0.622RH.P_{vs,inf}}{P_{atm} - RH.P_{vs,inf}}$$
$$C_{surf} = \frac{0.622a_w.P_{vs,surf}}{P_{atm} - a_w.P_{vs,surf}}$$
$$P_{vs,inf} = \exp\left(23.3265 - \frac{3802.7}{T_{inf}} - \left(\frac{472.68}{T_{inf}}\right)^2\right) \tag{22}$$
$$P_{vs,surf} = \exp\left(23.3265 - \frac{3802.7}{T} - \left(\frac{472.68}{T}\right)^2\right)$$

The effect of dew point temperature on moisture evaporation rate has been considered in the above equation. Thus; its value will be negative if the temperature of material surface is lower than the initial temperature.

The material deformation is due to moisture removal and there are no external forces at the exchange surface:

$$\sigma.n = 0 \tag{23}$$

7 Simulation

The numerical method used to solve this strongly coupled and nonlinear system was the finite element method (FEM). The heat, mass and momentum balances equations were implemented in a finite element solver and solved simultaneously. The Arbitrary Lagrange-Eulerian (ALE) formulation, as a method between the Lagrangian and Eulerian systems which combines them to solve the problem with moving boundaries such as drying process was used. The ALE is a finite element formulation in which the computational system is not a prior fixed in space (e.g. Eulerian-based finite element formulations) or attached to material (e.g. Lagrangian-based finite element formulations). ALE-based finite element simulations can alleviate many of the drawbacks that the traditional Lagrangian-based and Eulerian-based finite element simulations have. When using the ALE technique in engineering simulations, the computational mesh inside the domains can move arbitrarily to optimize the shapes of elements, while the mesh on the boundaries and interfaces of the domains can move along with materials to precisely track the boundaries. Simulation is carried out with a constant time step (dt =50 s). The physical and mechanical properties employed in simulation of the present study are summarized in Table 1.

Table 1   Clay properties used in the simulations

Property	Expression
Initial moisture content	$w_0 = 0.33 (kg/kgd . b)$
Critical moisture content	$w_{cr} = w_{sh} = 0.12 \ (kg/kgd . b)$
Equilibrium moisture content	$w_{eq} \approx 0.01$
Initial sample's temperature	$T_0 = 25^0 C$
Solid intrinsic density	$\rho_s^s = 2600 \ (kg/m^3)$
Intrinsic water density	$\rho_l^l = 1000 \ (kg/m^3)$
Solid specific heat	$Cp_s = 2000 \ (J/kg)$
Liquid specific heat	$C_{pl} = 4220 \ (J/kg)$
Solid thermal conductivity	$k_s = 1 \ (W/m \ K)$
Liquid thermal conductivity	$k_l = 0.597 \ (W/m \ K)$
Heat expansion coefficient [32]	$\alpha = 3*10^{-8}$
moisture expansion coefficient [42]	$\beta = 0.3$
Poisson's ratio [43]	$\nu = 0.4$
Young's modulus [43]	$E = 0.96\exp\left(\frac{1}{0.061+1.735w^{4.818}}\right) \ (Pa)$
Specific heat	$C_p = \frac{wC_{pl}+C_{ps}}{w+1} \ (J/kg)$
Density	$\rho = \frac{m_0(1+w)}{V(1+w_0)} \ (kg/m^3)$
Effective diffusion coefficient [44]	$D_{eff} = D_0 {}^* \left(\frac{T}{T_0}\right)^{a_T} {}^* \left(\frac{T}{T_0}\right)^{a_w}$ $D_0 = 7.36 {}^* 10^{-9} \ (m^2/s) \quad T_0 = 303 \ (k)$ $a_T = 9.5, \quad a_w = 0.5, \quad w_0 = 0.4 \ (kg/kgd.b)$

8 Material and experimental procedure

8.1 Material

All the clay-like material used for the experiment were extracted from clay deposit sites in Birjand -Iran. The chemical analysis and the Atterberg limits of the clay are given in Table 2 and Table 3, respectively.

8.2 Experimental equipment set-up

A laboratory chamber dryer was used for experimental study. A schematic of the experimental setup is shown in Fig. 2. The sample is located on a grid plate (holder) at the center of the dryer chamber. The holder is placed on the A&D GF3000 digital balance with 0.01 g resolution.

Table 2   Chemical analysis of the clay

element	percent
Si	59.5
Ca	7.83
Mg	4.20
Fe	4.50
Al	7.80
Ti, Mn	<1
L.O.I	9.80

The airflow generated by the blower passes through a controlled heating zone, enters the dryer chamber. In order to provide uniform drying conditions for all of the surfaces of the sample, the airflow enters both from the top and bottom and exits from the four vents located at the center of the all the lateral sides of the dryer chamber.

The temperature and relative humidity of the chamber are measured and logged in computer during drying by using a humidity temperature sensor (SHT25) connected to the national instrument USB-6009 data acquisition card. The measurement accuracy of the SHT25, is 0.2 °C and 1.8% for the temperature and the relative humidity, respectively.

The temperature and humidity are kept at set levels using feedback control. Also, the geometry variations of the sample were captured by using a digital camera. The chamber dryer equipped with two halogen lamps positioned at fixed location illuminating the scene evenly.

8.3 Model application to clay drying

The model developed was validated by comparing the model outputs (simulation results) with experimental results obtained from two sets of experiments in which different geometries and drying conditions are tested. The experiments were carried out in the laboratory chamber dryer.

In the first experiment, a cubic sample of clay material, with an approximate dimension of 7^*7^*5 cm was placed on the holder and the airflow circulated over the samples surface. The clay was mixed with water to make a workable paste with approximately 33% (dry basis). Then the clay paste was stored in an airtight container at room temperature (26 °C) for 48 h to make sure that the water content is uniform throughout the material providing a homogenized sample. The Cubic sample was dried at 100 °C with a relative humidity of 10%.

Table 3   Atterberg limits of the clay

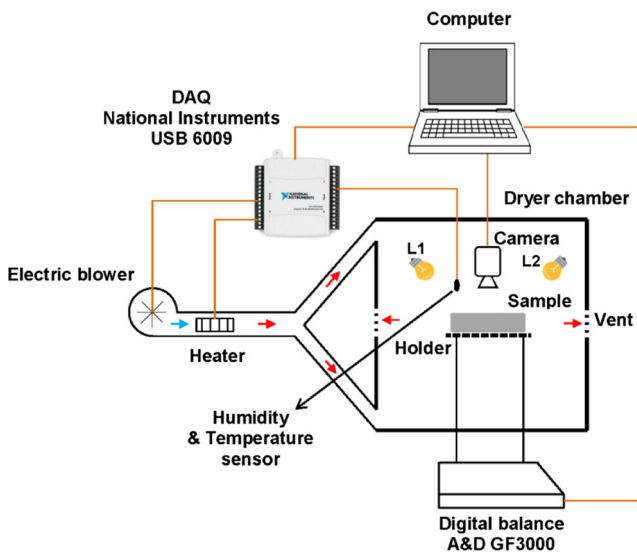| Atterberg Limits	moisture
Liquid limit	26%
Plastic limit	19%
Shrinkage limit (w_{sl})	12%

The drying process was controlled by a PC provided with the software and data acquisition card. During the experimental run the following parameters were controlled and recorded: drying time, air temperature, air relative humidity, geometry variations and mass of the sample. The mass evolution of the sample was logged into computer every 10 s by the precision digital balance.

During the experimental run, snapshots of the surface shrinkage of the top surface and one of side surfaces were taken every 15 min. Volumetric shrinkage of the sample was calculated using image processing techniques (Fig. 3).

Fig. 4 shows the comparison between the experimental results and the simulated values of the mean moisture contents evolution for clay sample. The sample is dried after about 12 h. The water vapor condenses onto the sample's surfaces at the beginning of drying, since for the chosen air conditions the dew point corresponds to 46 °C, which is greater than the sample's initial temperature of 26 °C. Consequently, the moisture content increases and a swelling of the medium occurs
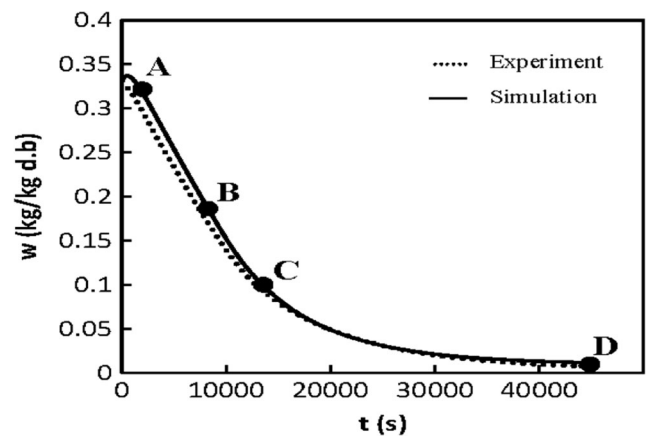

Fig. 4 Average moisture content changes

and continues until the dew temperature is reached when condensation stops. The points A, B, C and D in Figs. 4, 5, 6, 7, and 8 corresponds to the end of the preheating period, the end of the CDRP, the end of transition period and the end of FDRP, respectively.

Fig. 5 illustrates the evolution of the mean temperature inside the product. The temperature exhibits the classical evolution that occurs during convective drying. The three phases are clearly present: Phase 1 is the preheating period where the material is heated until its temperature reaches the wet bulb temperature (52 °C); Phase 2 is the CDRP, during which the diffusion of water from inside of the sample keeps up with the evaporation rate. The whole heat supplied by the air is consumed by the water evaporation at the surface and the temperature keeps constant. Phase 3, is the transition period and the FDRP, during which the temperature begins to grow with the time and trends to the drying air temperature.

According to the Atterberg limits in drying process, clay shrinks only when the moisture content is above shrinkage limit. In the current study the shrinkage limit and critical moisture content are assumed to be the same; ($w_{sh} = w_{cr} = 0.12 kg/kg$, d . b). This assumption has been made in other works dealing with clay material drying [46, 47]. Fig. 6 shows the
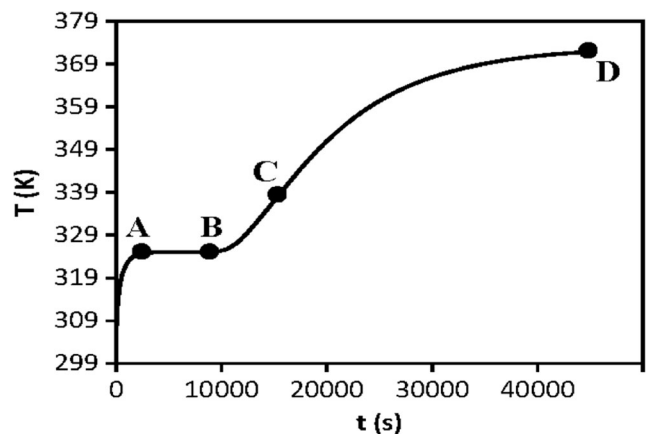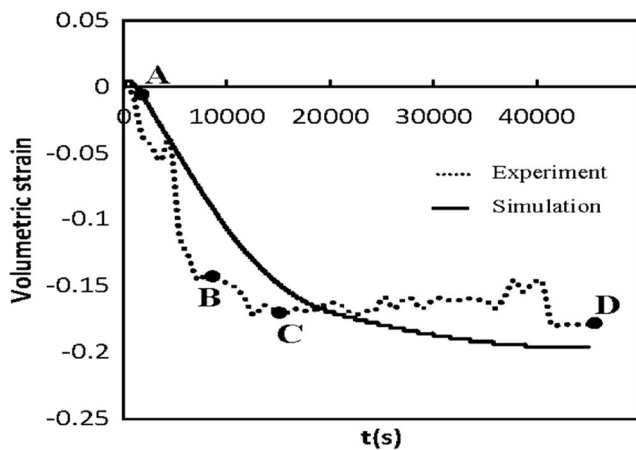

Fig. 3 Edge detection by image processing during the experiment run

Fig. 5 Average temperature changes

Fig. 6 Volumetric strain changes

Fig. 8 Clay density changes with time

comparison between the experimental results and the simulated values of the volumetric strain for clay sample. As seen from Fig. 4 the clay sample shrinks mainly in the preheating and constant rate periods, and during the falling drying rate period, the volume is approximately constant. The volumetric strain of the sample is about 17%.

The evaporation rate in the CDRP is supplied by the capillary flow from the material depth to the evaporation surface in porous clay-like material. During this period, evaporation occurs at the surface. At the critical moisture content, which is the end of the CDRP, evaporation rate starts to decrease because of the disconnection of the liquid meniscus from the surface and this decreasing trend continues until all the liquid meniscuses are disconnected. This period was termed as the transition period. Detachment of the last liquid meniscus from the surface marks the onset of the FDRP and changing the vaporization plane to a level below the surface [48].

The experimental results and the simulated values of the drying rate for clay sample are compered in Fig. 7. In the preheating period because of increase in sample temperature, drying rate increase until it reaches the wet bulb temperature; (point A). The CDRP begins from point A and drying rate
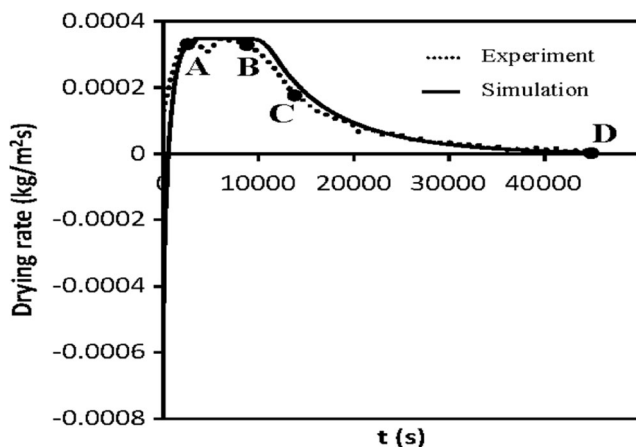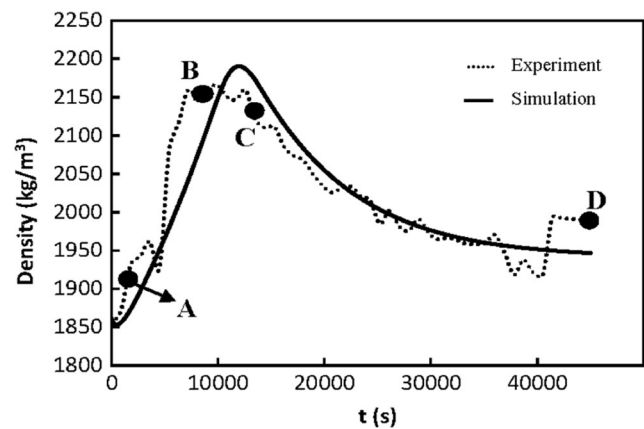

Fig. 7 Drying rate changes

remains constant. Moisture evaporation at exchange surface occurs with higher rates and values at edges. As soon as the first point moisture content of edge's point arrive at the shrinkage limits the transition period begins (point B) and because of the disconnection of the liquid meniscus from the surface the evaporation rate starts to decrease. At point C which is almost the inflection point, all liquid meniscuses have been disconnected and FDRP begins. Following disruption of hydraulic continuity between the sample depth and exchange surface liquid menisci recede into the porous medium and form a vaporization plane from which water vapor diffuses through the overlying dry layer to the exchange surface and then to the atmosphere [49].

Fig. 8 shows the comparison between the experimental results and the simulated values of the density for clay sample. It is important to note that the density increases at the beginning of drying, reaches a maximum at the time of 11,000 s which is almost the end of CDRP (point B) and then decreases. This evolution is the consequence of superposition of two phenomena: mass reduction and volume reduction. In preheating period and CDRP volume reduction is almost equal to the mass reduction (moisture removed by evaporation) from the sample (ideal shrinkage) [50]. Intrinsic clay density is more than water intrinsic density hence; the density increase until the end of CDRP. For moisture content below the critical limit the movement of the clay particles becomes more difficult and gradually the volume reduction stops. Therefore the effect of mass reduction dominates a decrease in the density. Similar results are reported in other works [46].

Fig. 9 shows the captured image of the sample surface during drying. Fig. 11a corresponds to the time that the moisture content at edge's point is just at the shrinkage limit and the CDRP has almost been ended. Fig. 11a corresponds to the point B in Figs. 6, 7, 8, 9, 10, and 11b shows the captured image of sample surface when it is in the transition period. During this period some of the liquid meniscuses are disconnected. The domain of not disconnected liquid meniscuses is approximately separated from other with a bound. Fig. 11c

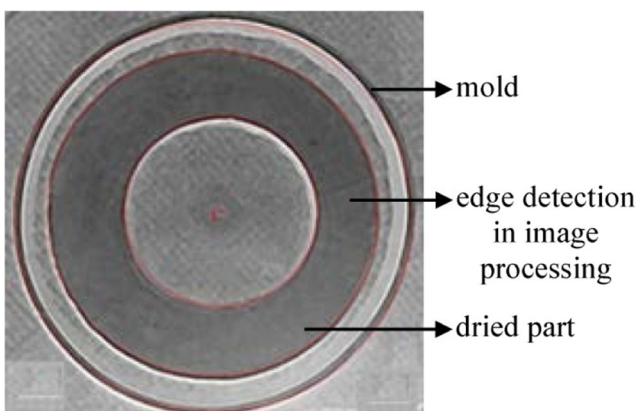a) t = 9000s   b) t = 10800s   c) t = 13500s
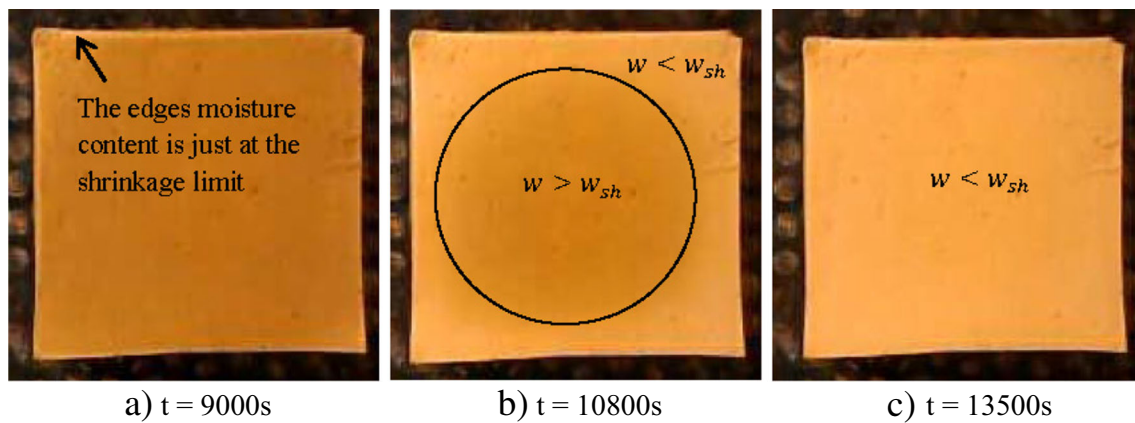
Fig. 9 the evolution of clay drying

shows the image taken at the end of transition period and the beginning of the FDRP when all the liquid meniscuses are disconnected and almost the sample stops to shrink. Fig. 11c corresponds to the point C Figs. 6, 7, 8, 9, and 10.

In the second experiment, a clay cylindrical sample of inside and outside diameter of 110 mm and 200 mm respectively, and thickness of 20 mm was used for experiment. The sample was dried at relative humidity of 25% and temperature of 30 °C. The volumetric and surface shrinkage of the dried product were measured by using image processing techniques. Red line in Fig. 10 shows the outside and inside edge of the dried product found by image processing techniques through edge detection algorithm. Table 4 compares the results of the volumetric shrinkage and outside diameter change of the dried product obtained experimentally with those obtained by simulation.

The experimental and numerical results for drying kinetic, volumetric strain, drying rate and density show a good agreement between each other. It shows that the developed mathematical model is accurate for the overall drying process. Therefor the simulation can be considered as a useful tool to predict the stresses induced by drying and the quality of dried product.

9 Initial condition effects on drying kinetic

In order to investigate the effects of material initial condition on the drying kinetic of the clay cylindrical sample, two series of simulation have been carried out. In the first series, the effects of different initial moisture contents and in the second series, the effects of different initial temperature on drying kinetic have been investigated.

Fig. 11 presents the evolution of the mean moisture content of a clay cylindrical sample with initial temperature of $25^{\circ}C$ and three different initial moisture contents of 20%, 30% and 40%. The temperature and relative humidity of the air in the simulation are assumed to be $70^{\circ}C$ and 20%, respectively. The dew point temperature for the chosen air conditions is about $36^{\circ}C$ which is higher than the initial temperature of the sample ($25^{\circ}C$). Hence the water vapor condenses on the surfaces of the sample. As a result, the moisture content of the sample increases and the sample starts to swell. The condensation phenomenon stops when the sample temperature reaches to the dew temperature.

Fig. 10 Dried part in laboratory
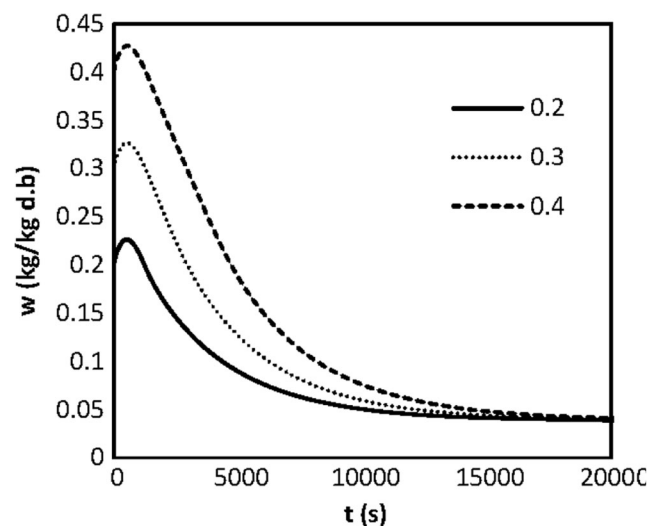
Fig. 11 Mean moisture evolution of the samples with different w_0

Table 4 Comparison of the experimental and simulation results

| parameter	simulation	image processing	error
external radius reduction	16.415 mm	16.646 mm	1.38%
volumetric shrinkage	30.136%	34.329%	12.21%

Fig. 12 illustrates the evolution of the mean temperature of the product which shows traditional periods of convective drying. The CDRP time increases for samples with more initial moisture contents because they have more potential to withstand the moisture evaporation rate from the exchange surface.

The stresses induced by drying are the result of non-uniform shrinkage. The evolution of drying induced stresses for the sample with initial moisture content and temperature of 30% and 25 °C respectively, at six points are shown in Fig. 13. The maximum stress happens in point 6 that is in the corner of the inner surface. The evolution of stress for the sample with different initial moisture content at point 6 is presented in Fig. 14. As one can see in Fig. 14, the maximum drying induced stress reduces in sample with lower initial moisture content since it faces less non uniform shrinkage.

The next series of simulation were carried out at afore mentioned drying condition for the samples with initial moisture content of 30% and five different initial temperature of 20^0C, 30^0C, 40^0C, 53^0C and 67^0C. Fig. 15 illustrates the evolution of the mean moisture content. This figure clearly shows the effect of initial temperature on material swelling because of vapor condensation in preheating period. Condensation phenomena appears in samples with initial temperature of 20^0C and 30^0C which are lower than the dew point temperature of chosen air condition $(36^\circ C)$.The mean temperature evolution of the samples are presented in Fig.
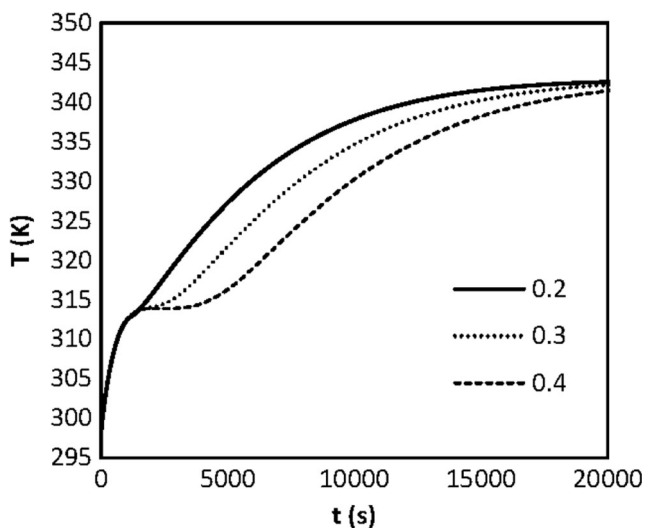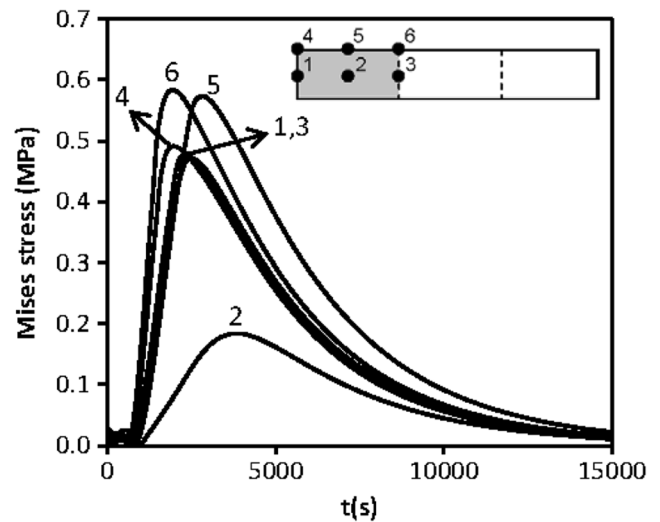
Fig. 13 Drying induced stress at six points

16, each of which shows the traditional periods that occur during convective drying and reaches the wet bulb temperature at CDRP. The heat and mass transfer rate are different for each initial temperature; consequently the wet bulb temperature is different in samples with different initial temperature. Fig. 17 shows the evolution of drying induced stress of samples at point 6. By increasing the initial temperature, the maximum stress and the occurrence time decrease. The maximum stress of samples with initial temperature of 20^0C and 67^0C is about 602 KPa and 401 KPa, respectively which is reduced by about 44%. Drying induced stresses indicates the possibility of the material fracture. This is a great value compared even with the newly developed techniques, namely the intermittent drying in which claims of 29% reduction on stresses are reported [Manel et al. 2014]. Energy requirements for increasing initial temperature are

Fig. 12 Temperature evolution of the samples with different w_0
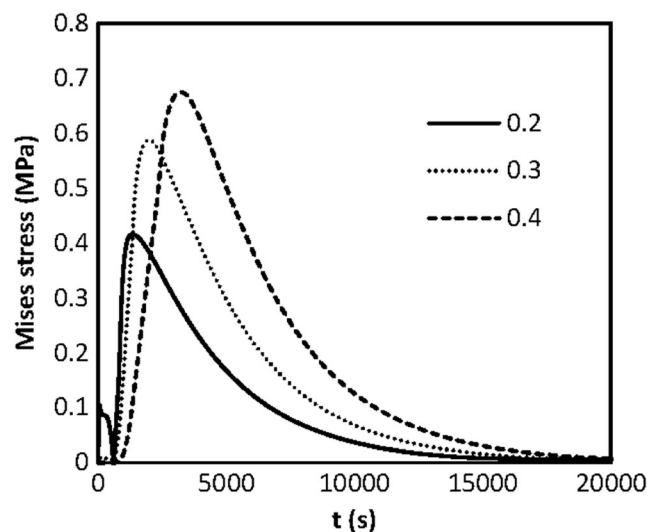
Fig. 14 Drying induced stresses of the samples with different w_0

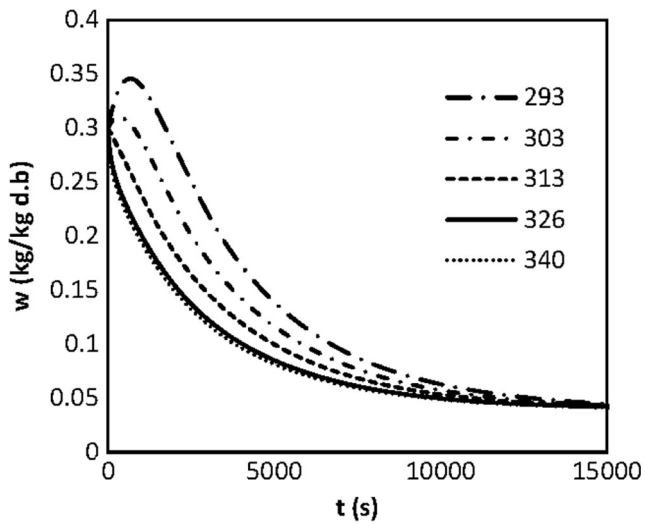Fig. 15 Mean moisture evolution of the samples with different T_0

Fig. 17 Drying induced stresses of the samples with different T_0

almost equal to the preheating period of drying process which the sample temperature increases to the wet bulb temperature. Preheating period often represents a negligible proportion of the overall drying process [5, 51]. So it can be concluded that energy requirements for increasing initial temperature are negligible to the overall drying energy consumption. Energy consumption of intermittent drying with periodically air temperature is less than continuous drying. But Energy consumption of intermittent drying with periodically air humidity is more [52]. It's important to note that intermittent drying is difficult to operate in comparison with continuous drying and also need drying process modeling and simulation in order to design operation schedule. Not well designed schedule of application of the intermittent condition may made the stress filed induced by drying worse [53].hence; Increasing the initial temperature of the material in comparison to the intermittent drying is easier either in
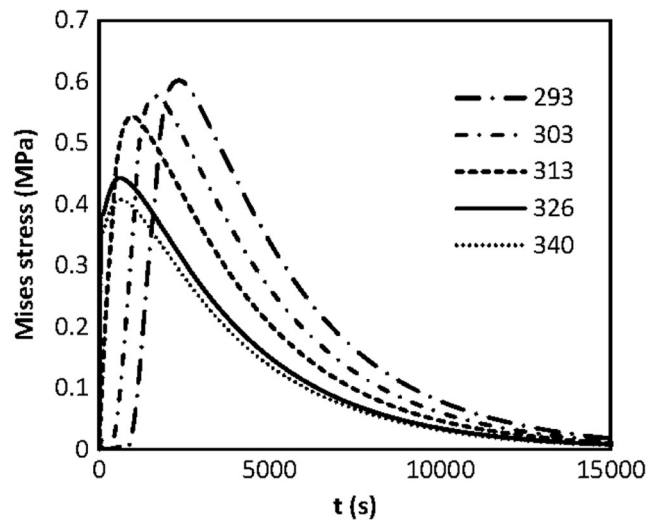
terms of design or in terms of implementation and can be considered as an efficient method in order to reduce the drying induced stresses.

The occurrence time of maximum stress of samples with initial temperature of 20^0C and 67^0C are about 2400 s and 650 s, respectively. Decreasing the occurrence time of maximum stress makes the application of more sever condition in the rest of drying process possible, hence; decreased drying time.

The most important effect of the shrinkage on drying kinetic is the change of drying surface that changes the drying rate. Fig. 18 shows both cases of considering and not considering the shrinkage in the mean moisture content evolution. It can be seen that not considering the deformation at the early stage of drying process reduces the drying rate (detail A) since the condensation phenomenon described in previous section causes swelling of medium and provides more evaporation surface. As a result of material shrinkage, the evaporation
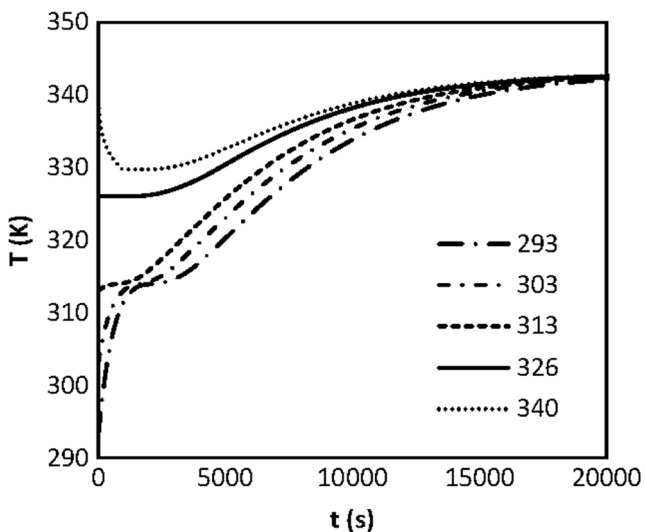

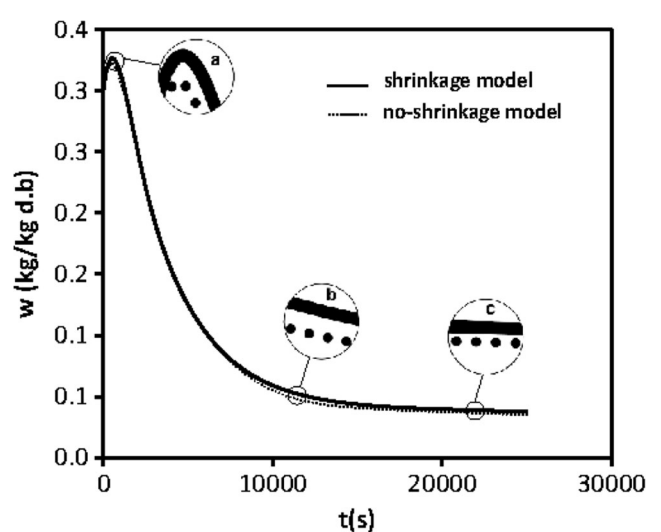Fig. 16 Temperature evolution of the samples with different T_0

Fig. 18 Effect of shrinkage on the drying behavior

surface reduces in CDRP. Consequently, not considering the deformation increases the drying rate (detail B). The difference between the two curves remains approximately stable since the start of FDRP. This is due to the fact that in FDRP, the drying rate is fully governed by the internal moisture diffusion rate and not by the evaporation rate (detail C). The same results have been reported in other studies [30].

10 Conclusions

A fully coupled model was established to foresee the stress and strain behavior of clay like material with respect to the initial conditions of material. The numerical method used to solve this strongly coupled and nonlinear system was the finite element method. The experimental and numerical results for drying kinetic, volumetric strain and drying rate show a good agreement between to each other. It shows that the developed mathematical model is accurate for overall drying process.

The comparison of drying induced stresses in samples with different initial moisture content led us to conclude that reducing the initial moisture content reduces the generated stresses within dried material without substantial change in drying time. Also the investigation of drying induced stresses in samples with different initial temperature leads to the conclusion that increasing the initial moisture content reduces the stresses generated, making it possible to produce parts with less stress/strain based defects such as cracks and deformation.

The amount of the maximum stress reduction by increasing the initial temperature from 20^0C to 67^0C is almost equals to the maximum stress reduction of well scheduled intermittent drying in comparison to the stationary drying.

Also the influence of material shrinkage on drying kinetic was studied. Predicted drying curves with and without including the shrinkage effect show that not considering the shrinkage at the early stage of drying reduces the drying rate however; the drying rate increases in the constant drying rate period. The difference between the two curves becomes relatively stable by starting the period of falling drying rate since in this period, drying rate is governed by the internal moisture diffusion rate and not by evaporation rate.

α, Thermal Expansion coefficient; β, Shrinkage coefficient; ε, strain; λ , μ, Lame constants; ν, Poisson's ratio; σ, Stress (Pa); C_p, heat capacity $(J\,kg^{-1}K^{-1})$; D, Diffusion coefficient (m^2s^{-1}); E, Young modulus (Pa); F_m, Rate of moisture vaporization $(kg\,m^{-2}s^{-1})$; h, Convection coefficient $(Wm^{-2}K^{-1})$; h_v, Latent heat of evaporation $(J\,kg^{-1})$; k, Thermal conductivity $(Wm^{-1}K^{-1})$; K, Bulk modulus; P, pressure (Pa); RH, Relative humidity of air $(kg\,kg^{-1})$; t, Time (s); T, Temperature (K); w, Moisture content $(kg\,kg^{-1}\,d\,.\,b)$

inf, Ambient air; l, Liquid; s, Solid; *surf*, Evaporation surface; *vs*, Saturated vapor.

References

1. Liu X, Lee DJ (2015) Some recent research and development in drying technologies: product perspective. Dry Technol 33:1339–1349
2. Musielak G, Mierzwa D (2009) Permanent strains in clay-like material during drying. Dry Technol 27:894–902
3. Khalili K, Ahmadi-Brooghani SY, Bagherian M (2014) Experimental and numerical study of the ceramic drying process and cracking. J Solid Fluid Mech 4:119–129
4. Heydari M, Khalili K (2016) Investigation on the effect of Young's modulus variation on drying-induced stresses. Transp Porous Med 112:519–540
5. Kowalski SJ (2003) Thermomechanics of drying processes. Springer-Verlag, Berlin Heidelberg
6. Vasić M, Grbavčić Ž, Radojević Z (2014) Determination of the moisture diffusivity coefficient and mathematical modeling of drying. Chem Eng Process Process Intensif 76:33–44
7. Islam MR, Mujumdar AS (2003) Role of product shrinkage in drying rate predictions using a liquid diffusion model. Int Commun Heat Mass Transfer 30:391–400
8. Silva WP, da Silva CMDP, da Silva LD, Farias VSO (2013) Drying of clay slabs: experimental determination and prediction by two-dimensional diffusion models. Ceram Int 39:7911–7919
9. Efremov GI (2002) Drying kinetics derived from diffusion equation with flux-type boundary conditions. Dry Technol 20:55–66
10. da Silva WP, de Oliveira Farias VS, de Araújo Neves G, de Lima AGB (2012) Modeling of water transport in roof tiles by removal of moisture at isothermal conditions. Heat Mass Transf 48:809–821
11. Mihoubi D, Bellagi A (2009) Stress generated during drying of saturated porous media. Transp Por Med 80:519–536
12. Oztop HF, Akpinar EK (2008) Numerical and experimental analysis of moisture transfer for convective drying of some products. Int Commun Heat Mass Transfer 35:169–177
13. Esfahani JA, Majdi H, Barati E (2014) Analytical two-dimensional analysis of the transport phenomena occurring during convective drying: apple slices. J Food Eng 123:87–93
14. Lewis RW, Strada M, Comini G (1977) Drying-induced stresses in porous bodies. Int J Numer Methods Eng 11:1175–1184
15. Kowalski SJ, Pawlowski A (2010) Modeling of kinetics in stationary and intermittent drying. Dry Technol 28:1023–1031
16. Kowalski SJ, Szadzińska J (2012) Non-stationary drying of ceramic-like materials controlled through acoustic emission method. Heat Mass Transf 48:2023–2032
17. Itaya Y, Okouchi K, Mori S (2001) Effect of heating modes on internal strain-stress formation during drying of molded ceramics. Dry Technol 19:1491–1504
18. Banaszak J, Kowalski SJ (2005) Theoretical and experimental analysis of stresses and fractures in clay like materials during drying. Chem Eng Process Process Intensif 44:497–503
19. Musielak G (2000) Influence of the drying medium parameters on drying induced stresses. Dry Technol 18:561–581
20. Manel BA, Mihoubi D, Jalila S, Ahmed B (2014) Strain–stress formation during stationary and intermittent drying of deformable media. Dry Technol 32:1245–1255
21. Augier F, Coumansa WJ, Hugget A, Kaasschieter EF (2002) On the risk of cracking in clay drying. Chem Eng J 86:133–138
22. Khalili K, Heydari M (2012) Studying the effect of part thickness on cracking during drying process. J Modares Mech Eng 12:103–116
23. Pourcel F, Jomaa W, Puiggali JR, Rouleau L (2007) Criterion for crack initiation during drying: alumina porous ceramic strength improvement. Dry Technol 172:120–127
24. Mermerdaş K, Güneyisi E, Gesoğlu M, Özturan T (2013) Experimental evaluation and modeling of drying shrinkage

behavior of metakaolin and calcined kaolin blended concretes. Constr Build Mater 43:337–347

25. Musielak G, Śliwa T (2015) Modeling and numerical simulation of clays cracking during drying. Dry Technol 33:1758–1767

26. Belleghem MV, Steeman M, Janssen H, Janssens A, Paepe MD (2014) Validation of a coupled heat, vapour and liquid moisture transport model for porous materials implemented in CFD. Build Environ 81:340–353

27. Chemkhi S, Zagrouba F (2005) Water diffusion coefficient in clay material from drying data. Desalination 18:491–498

28. Musielak G, Kieca A (2009) Temperature dependence of the moisture diffusion coefficient in a high moisture content material. Chem Process Eng 30:231–242

29. Mujumdar AS, Devahastin S (2000) Fundamental principles of drying. Exergex, Brossard

30. Ketelaars AAJ (1993) Drying Deformable Media, Kinetics, Shrinkage and Stress. PhD Thesis. Eindhoven, University of Eindhoven

31. Kowalski SJ (2000) Rate of drying and stresses in the first period of drying. Dry Technol 18:583–600

32. Banaszak J, Kowalski SJ (2002) Drying induced stresses estimated on the base of elastic and viscoelastic models. Chem Eng J 86:139–143

33. Heydari M, Khalili K (2015) Modeling enhancement and simulation of distortion in drying process. J Modares Mech Eng 15:291–301

34. Sonntag RE, Borgnakke C, Van Wylen GJ, Van Wyk S (1998) Fundamentals of thermodynamics, vol 6. Wiley, New York

35. Stull R (2011) Wet-bulb temperature from relative humidity and air temperature. J Appl Meteorol Climatol 50:2267–2269

36. Brosnan DA, Robinson GC (2003) An introduction to drying of ceramics. The American Ceramic Society, Westerville

37. Khalili K, Heydari M (2014) Drying clay bricks with variable Young's modulus. Procedia Technol 12:382–387

38. Kowalski SJ (2001) Thermomechanical approach to shrinking and cracking phenomena in drying. Dry Technol 19:731–765

39. Couture F, Laurent S, Roques MA (2007) Drying of two-phase media: simulation with liquid pressure as driven force. AICHE J 53:1703–1717

40. Kowalski SJ, Rybicki A (2007) The vapour–liquid interface and stresses in dried bodies. Transp Porous Med 66:43–58

41. Kowalski SJ, Banaszak J, Rybicki A (2010) Plasticity in materials exposed to drying. Dry Technol 65:5105–5116

42. Mihoubi D, Bellagi A (2012) Modeling of heat and moisture transfers with stress–strain formation during convective air drying of deformable media. Heat Mass Transf 48:1697–1705

43. Chemkhi S, Jomaa W, Zagrouba F (2009) Application of a coupled thermo-hydro-mechanical model to simulate the drying of non-saturated porous media. Dry Technol 27:842–850

44. Mujumdar AS (2006) Handbook of industrial drying, third edn. CRC press, Boca Raton

45. Khalfaoui K, Chemkhi S, Zagrouba F (2013) Modeling and stress analysis during drying of a deformable and saturated porous medium. Dry Technol 31:1124–1137

46. Hammouda I, Jlassi K, Mihoubi D (2015) Changes in the physicomechanical characteristics of a ceramic paste during drying. Comptes Rendus Mécanique 343:419–428

47. da Silva WP, da Silva LD, de Oliveira Farias VS, da Silva CMDP (2013) Water migration in clay slabs during drying: a three-dimensional numerical approach. Ceram Int 39:4017–4030

48. Shokri N, Or D (2011) What determines drying rates at the onset of diffusion controlled stage-2 evaporation from porous media?. Water Resour Res 47:1–8

49. Shokri N, Lehmann P, Or D (2009) Critical evaluation of enhancement factors for vapor transport through unsaturated porous media. Water Resour Res 45:1–9

50. Couture F, Laurent S, Roques MA (2007) Drying of two-phase media: simulation with liquid pressure as driven force. AICHE J 53(7):1703–1717

51. Dincer I, Zamfirescu C (2015) Drying phenomena: theory and applications. John Wiley & Sons, Hoboken

52. Kowalski SJ, Pawłowski A (2011) Intermittent drying of initially saturated porous materials. Chem Eng Sci 66(9):1893–1905

53. Itaya Y, Mori S, Hasatani M (1999) Effect of intermittent heating on drying-induced strain-stress of molded clay. Dry Technol 17(7–8):1261–1271